Polymer Degradation and Stability 166 (2019) 50–59

Contents lists available at ScienceDirect

Polymer Degradation and Stability

journal homepage: www.elsevier.com/locate/polydegstab

In situ prepared polyamide 6/DOPO-derivative nanocomposite for melt-spinning of flame retardant textile filaments

Jelena Vasiljević [a, *], Marija Čolović [b], Ivan Jerman [b], Barbara Simončič [a], Andrej Demšar [a], Younes Samaki [c], Matic Šobak [b], Ervin Šest [b], Barbara Golja [a], Mirjam Leskovšek [a], Vili Bukošek [a], Jožef Medved [a], Marco Barbalini [d], Giulio Malucelli [d], Silvester Bolka [e]

[a] University of Ljubljana, Faculty of Natural Sciences and Engineering, Aškerčeva 12, 1000, Ljubljana, Slovenia
[b] National Institute of Chemistry, Hajdrihova 19, 1000, Ljubljana, Slovenia
[c] Université Grenoble Alpes, Polytech Grenoble, 621 Avenue Centrale, 38400, Saint-Martin-d'Hères, France
[d] Politecnico di Torino, Department of Applied Science and Technology, Viale Teresa Michel 5, 15121, Alessandria, Italy
[e] Faculty of Polymer Technology, Ozare 19, 2380, Slovenj Gradec, Slovenia

ARTICLE INFO

Article history:
Received 28 February 2019
Received in revised form
7 May 2019
Accepted 9 May 2019
Available online 13 May 2019

Keywords:
Polyamide 6
DOPO derivative
Flame retardant
In situ polymerization
Melt-spinning
Nanocomposite filament yarns

ABSTRACT

A novel flame retardant polyamide 6 (PA6)/bridged 9,10-dihydro-9-oxa-10-phosphaphenanthrene-10-oxide (DOPO)-derivative (PHED) nanocomposite textile filament yarns were developed. The scalable production approach includes *in situ* water-catalyzed ring-opening polymerization of ε-caprolactam in the presence of the flame retardant PHED followed by melt-spinning of nanocomposite filament yarns and production of knitted fabrics. The specific chemical structure of the PHED additive enabled its excellent miscibility with molten ε-caprolactam and the uninterrupted polymerization of ε-caprolactam. The produced PA6/PHED nanocomposite was characterized by the preserved molecular structure of the polyamide 6 and uniformly distributed nano-dispersed FR at concentrations of 10 and 15 wt %. The PA6/PHED nanocomposite structure was successfully preserved after the melt-spinning processing. The PA6 nanocomposite filament yarns at the applied 15 wt %. loading of PHED showed (a) increased thermo-oxidative stability compared to neat PA6 up to 500 °C, with a 43% higher residue at 500 °C and (b) self-extinguishment of fiber strand and knitted samples within 1 s in standard vertical flame spread tests (ASTM D6413), followed by the significant reduction of the melt-dripping and the melt-drop flammability. Additionally, 1.2 mm-tick PA6/PHED bar samples achieved a V0 rating in UL94 vertical burning test at the applied 10 wt % concentration of PHED. This innovative and scalable approach could pave the way for the production of new-generation nanocomposite PA6 filament yarns with self-extinguishing properties at the macro-scale, which would be highly beneficial for increasing fire safety, whilst maintaining the use of a DOPO derivative at the minimum level.

1. Introduction

The PA6 textile materials are widely used as automotive and home textiles, for upholstering furniture and carpets. However, retardation of the combustion of polyamide 6 (PA6) textile materials remains an important social and scientific problem due to the rapidly growing demand for a safer environment [1–3]. The PA6 textiles represent a sizable fraction of the total volume of synthetic textile materials and have an exceptional and rare feature, i.e., their chemical recyclability back into monomer ε-caprolactam, which is of high importance for the future preservation of limited petroleum resources and the reduction of global environmental pollution [4,5]. The commonly used approach for the development of inherently flame retardant (FR) PA6 fibers is based on the use of melt-compounded PA6/FR composites in the melt-spinning process [6–11]. To this purpose, phosphorus (P)-, and nitrogen (N)-based FRs, inorganic FRs and their mixtures have been used as the most prominent alternatives to their toxic and bio persistent halogenated counterparts [12–14]. Since thin yarn and fabric structures with much higher surface-to-volume ratio than that of bulk plastics also have intensified burning rates, an increased concentration of P/N FRs is unavoidable to achieve effective flame retardancy.

* Corresponding author.
E-mail address: jelena.vasiljevic@ntf.uni-lj.si (J. Vasiljević).

https://doi.org/10.1016/j.polymdegradstab.2019.05.011
0141-3910/

However, the essential obstacle of this approach is that FR concentrations higher than 10 wt % worsen spinnability, cause clogging of filters and spinnerets, and significantly impair the tensile properties of the resulting filaments [3,6,9]. This is the most important limitation in the production of FR PA6 fibers in comparison with PA6 bulk plastic materials [15–17]. Consequently, concentrations of P/N FR additives that are adequate for continuous melt-spinning with acceptable reduction of the tensile properties provide only a poor FR effect.

The origin of the problem described above is the high melt reactivity of PA6, which causes poor dispersion of FRs and the production of only micro-grade dispersed composites [18]. In parallel, the most advanced research in the field of PA6 nanocomposites with incorporated nanocarbon materials, nanoclays and other inorganic particles confirms *in situ* polymerization as a successful method for controlling the size of the incorporated additives at the nano level [19–23]. Despite this, the *in situ* polymerization of ε-caprolactam remains almost unexploited method for the production of PA6 nanocomposites with P/N FRs. The first scientific research employing the *in situ* polymerization of ε-caprolactam dates from 1986, when Alfonso et al. reported that this method enabled obtaining a homogeneous dispersion using red P, MgO and Dechlorane plus within the PA6 matrix, with enhanced fire performance of the compression-molded plastic [24]. The Toyota group designed an *in situ* polymerization strategy for the production of PA6 nanocomposites with inorganic additives [25]. This strategy was successfully applied to different polymers and inorganic additives. More recent studies reported on the successful *in situ* polymerization ε-caprolactam carried out in the presence of adipic acid-melamine salt and cyanuric acid-hexane diamine, which provided enhanced flame retardancy of the bar nanocomposite samples [26,27]. However, the behavior of knitted fabrics in contact with flame was discussed only qualitatively [27].

The usefulness of nanocomposite systems is determined by their ability to retain the nano-dispersed structure after melt-processing, e.g. melt-spinning. The first essential issue to be considered is the use of FR compound, which chemical structure should allow the unhindered incorporation of the nano-dispersed FR into the PA6 matrix during the polymerization process, with minimal impact on the structure and length of the PA6 chains and the polymer crystallinity. The second essential issue to be considered is the requirement that the chemical structure of the FR compound must have specific pyrolysis characteristics, which will provide flame retardancy protection of PA6 at the specific decomposition temperature [3,13]. According to the literature, there is a phosphorus flame retardant, based on bridged 9,10-dihydro-9-oxa-10-phosphaphenanthrene-10-oxide (DOPO), i.e., 6, 6'-(1-phenylethane-1,2-diyl)bis (dibenzo [c,e] [1,2]-oxaphosphinine-6-oxide) (PHED), whose pyrolysis specifics could provide effective production of volatile radical scavengers at temperatures that match the decomposition temperatures of PA6 [28]. Additional advantages of the chemical structure of PHED are (a) the absence of chemical groups, which could potentially chemically interact during the polymerization process and (b) a melting point (equal to approximately 187 °C) lower than the temperatures of PA6 polymerization and melt processing, which may be beneficial for uniform nanodispersion of the additive in the molten ε-caprolactam and, afterwards, in the PA6 matrix. Until now, this FR molecule found its application in poly (lactic acid) and epoxy resin composites and has never been exploited for the production of PA6 composites [28,29].

In this work, we successfully produced halogen-free and highly effective flame retardant PA6/FR nanocomposite filament yarns by incorporating the PHED additive into the PA6 matrix during the *in situ* water-catalyzed ring-opening polymerization of ε-caprolactam. This paper presents the first-ever study of the thermal stability and flame retardancy of PA6/bridged DOPO derivative nanocomposite filament yarns, along with their physical and mechanical properties. The flame retardancy performance of the bulk plastic or fibrous nanocomposite systems were evaluated, wherein overlapping of the additive and polymer decomposition temperatures is maximized and the FR decomposition products mainly act in the gas phase.

2. Experimental

2.1. Materials

ε-Caprolactam was kindly supplied by AquafilSLO d. o.o., Slovenia. 9,10-dihydro-9-oxa-10-phosphaphenanthrene-10-oxide (DOPO) and phosphorus oxychloride, 2-acetophenon, xylene and isopropyl alcohol were purchased from Sigma Aldrich. 6, 6'-(1-phenylethane-1,2-diyl)bis (dibenzo [c,e] [1,2]-oxaphosphinine-6-oxide) flame retardant (PHED) was synthesized according to the literature [30]. Structure of the PHED additive was confirmed by ^{1}H and ^{31}P NMR spectroscopy measurements (Fig. S1).

2.2. Nanocomposite production

Nanocomposites were prepared by the *in situ* water-catalyzed ring-opening polymerization of the ε-caprolactam monomer in the presence of PHED. The polymerization process was performed in the hydrothermal autoclave reactor with a Teflon chamber. First, vacuum-dried ε-caprolactam monomer was melted in the Teflon chamber at 180 °C on a temperature-controlled hot plate provided with magnetic stirrer and placed inside a fume hood under an inert argon atmosphere. The PHED additive was dispersed in the molten ε-caprolactam at concentrations of 10 and 15 wt % under constant stirring until a transparent melt was obtained. Subsequently, the temperature was gradually reduced to 80 °C, and then 1 wt % of water was added dropwise. Afterwards, the Teflon chamber was placed in the hydrothermal autoclave reactor, and the mixture was polymerizing at 250 °C for 10 h under autogenous pressure. For comparison, the PA6 sample in the absence of PHED was synthesized through the same method. The ground plastic materials were subjected to vacuum-drying at 80 °C for 24 h before further processing. The resulting nanocomposite materials containing PHED at concentrations of 10 and 15 wt % were coded as PA6/10PHED and PA6/15PHED, respectively.

2.3. Melt-spinning and fabric knitting

PA6, PA6/10PHED and PA6/15PHED nanocomposite filament yarns were produced using the laboratory-scale melt-spinning and drawing device (Extrusion System Ltd, Bradford, Great Britain). The temperature of an extruder (three zones), metering pump, and spin-pack (two zones) was set to 210 °C. The extruder screw speed was 1.5 rpm. The spinneret for multifilament spinning had 10 holes with diameters of 0.35 mm. The extruded filaments were quenched in the air at room temperature and were wound using a winder operating at a 120 m min^{-1} speed with no filament breakage. The melt-spinning process was conducted without clogging of the filters and spinneret. PA6, PA6/10PHED and PA6/15PHED knitted fabric samples with the right-right structure were produced on a hand knitting machine RIMACH operating with 10-gauge needles. For each sample, three multifilament yarns were used for knitting yielding the area density of approximately 300, 400 and 360 g m^{-2} for PA6, and PA6/10PHED and PA6/15PHED samples, respectively. Fig. 1 shows the production route for the FR PA6 nanocomposite filament yarns and fabric, and the optical microscopy and SEM

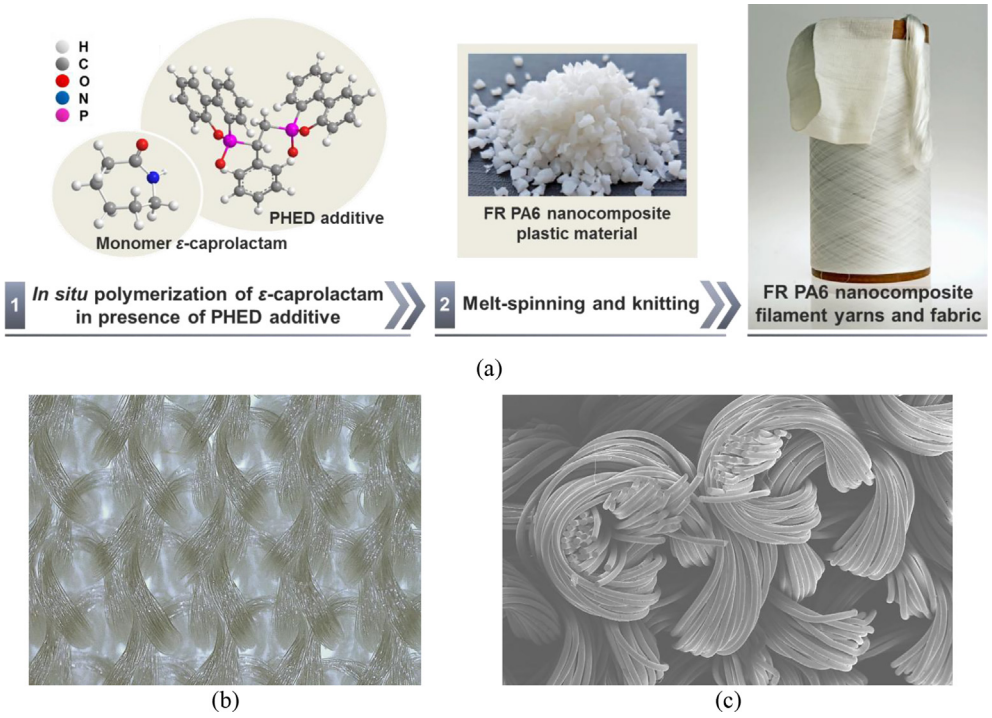

Fig. 1. Production route for FR PA6 nanocomposite filament yarns and fabric (a), the optical microscopy (a) and SEM images (b) of knitted fabric corresponding to the PA6/15PHED sample.

images of the PA6/15PHED knitted fabric structure.

2.4. Characterization

Scanning electron microscopy (SEM) and energy-dispersive X-ray spectroscopy (EDS) were performed on a SEM Cambridge 360 microscope equipped with an energy dispersive X-ray spectrometer (EDS) INCA 250. The samples were coated with Au. Differential scanning calorimetric (DSC) analysis was used to measure the melting (T_m) and crystallization (T_c) temperatures using an STA 449c Jupiter instrument (NETZSCH) at temperatures ranging from 0 to 300 °C with heating and cooling rates of 10 °C min^{-1} in a nitrogen atmosphere. An X-ray diffractometer (XRD) PANalytical X'Pert PRO (CuKα1 = 1.5406 Å) with a completely open X'Celerator detector (2.122° 2 θ) was used for recording the XRD pattern of polyamide 6. The XRD pattern was measured from 5 to 80° 2θ with a step size of 100 s. Dynamic-mechanical analysis (DMA) was performed on a TA instrument (DMA Q800, TA Instruments) with a controlled gas cooling accessory. The dimensions of the samples were 12.5 × 0.5 cm^2. The samples were heated from 0 to 160 °C at a constant rate of 3 °C min^{-1}. During heating, the test samples were deformed (oscillated) at constant amplitude (strain) of 8 μm and a frequency of 10 Hz. The tensile properties were analyzed with an Instron 5567 dynamometer in accordance with SIST ISO 2062:1997. The method was adjusted so that the gauge length was 100 mm and the deformation rate was 350 mm min^{-1}. Rheological measurements of the melts were conducted on a Physica MCR 301 rotational rheometer (Anton Paar), using a parallel-plate geometry with a diameter of 25 mm and a gap of 0.5 mm. The measurement temperature was 220 °C, with a fixed shear strain of 5% and over a frequency range of 0.01–100 rad s−1. Thermogravimetric (TG) analyses in an air and nitrogen atmospheres were performed on a STA 449c Jupiter instrument (Netzsch) and a TA Instruments SDT 2960, respectively, from 50 to 800 °C with heating and cooling rates of 10 °C min^{-1} in open alumina pans. Alternatively, TGA (SDT 2960, TA Instruments) was coupled with infrared spectroscopy (Nicolet iS10 by Thermo-Scientific); these analyses were carried out in a nitrogen atmosphere. The UL-94 test (Underwriters Laboratory) was performed in a vertical configuration. The size of the hot-pressed bar samples was 125 × 13 × 1.2 mm^3. Five measurements were made for each sample. The standard vertical flame spread test (ASTM D6413) was performed on the fiber strand and knitted fabric samples. The fiber strand samples (approximately 12.5 cm long, 1.5 cm wide, and 1.2 cm thick) were prepared by twisting several filaments together. The size of the tested surface area of the fabric samples was 150 × 50 mm^2 because of the limited quantities of the fabrics available. Additionally, the cotton indicators positioned below the fiber strand and knitted fabric samples in accordance with the standard UL 94 were used in order to evaluate the flammability of the melt-drips. Cone calorimetry (Fire Testing Technology, FTT) tests were performed using square samples (100 × 100 cm^2) under an irradiative heat flux of 35 kW/m^2 in a horizontal configuration. The fabrics were placed in a sample holder and maintained in the correct configuration by a metallic grid. Time to ignition (TTI), heat release rate (HRR), total heat release (THR), the peak of HRR (PHRR) and time (tPHRR), effective heat of combustion (EHC) and residue were measured. Total smoke release (TSR), the average specific extinction area (SEA), CO and CO_2 yield ([CO] and [CO_2]) were evaluated, as well.

3. Results and discussion

3.1. Structure characterization and mechanical properties

SEM images and EDX elemental distribution maps of phosphorus for the surfaces and cross-sections of the PA6 and the PA6/10PHED and PA6/15PHED nanocomposite filament samples are shown in Fig. 2.

Visual observation and EDX elemental mapping revealed that phosphorus was uniformly distributed on the surface and in the

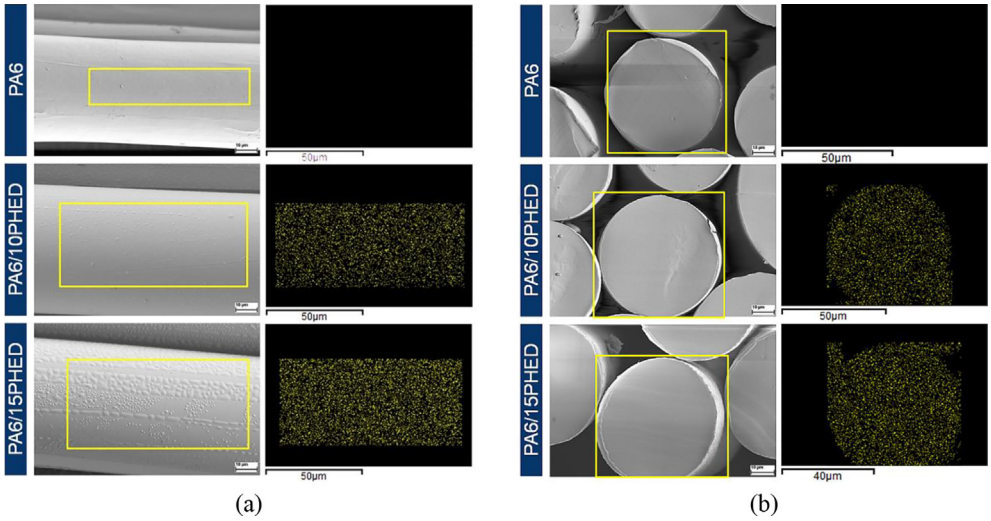

Fig. 2. SEM and EDX phosphorus mapping of the filament (a) surface and (b) cross-section for the PA6, PA6/10PHED and PA6/15PHED filament samples.

fiber bulk, as were carbon and oxygen (Fig. S2). These results confirmed the uniformly distributed nano-dispersed PHED additive in the nanocomposite, as well as the stability of the produced nanocomposite to preserve such structure after the melt-spinning process. The absence of possible agglomerates in the elemental distribution maps confirmed that the axially oriented "bumps" visible in the SEM images of the nanocomposite fibers surfaces were not PHED agglomerates but were formed during the melt-spinning.

These results confirmed the production of unique FR PA6 nanocomposite filament yarns. The preservation of the nanocomposite structure in the PA6/10PHED and PA6/15PHED filaments indicates the achievement of a kinetically trapped nanostructure with favorable thermodynamics to retain the achieved dispersed structure upon the application of melt-spinning conditions.

The crystallization (T_c) and melting (T_m) temperatures (Fig. 3a and b) of the PA6/10PHED and PA6/15PHED filament samples were only a few degrees lower compared to that of the PA6. Accordingly, the drop of the T_c to 6.5 °C and 7.1 °C for PA6/10PHED for PA6/15PHED, respectively, suggests that incorporated PHED additive only slightly hinders polymer crystallization. The T_m values of the nanocomposites are within the melting range of PA6 (215–228 °C), and a slight decrease of the T_m confirmed that PHED minimally affects the concentration of amide groups and the number of CH_2 groups linked to the latter. This confirmed that PHED additive minimally affected the polymerization process and polymer molecular structure. Apparently, good miscibility between the PHED additive and ε-caprolactam melt enabled unhindered polymerization with simultaneous uniform incorporation of the nano-dispersed PHED into the PA6 matrix.

The normalized heights of the diffraction peak maxima obtained by the XRD analysis of the PA6 and the PA6/10PHED and PA6/15PHED nanocomposite filament samples are presented in Fig. 4.

The XRD patterns confirmed the successful retention of the dominant monoclinic α crystal form. Namely, the two diffraction peak maxima of the PA6 fiber sample were located at $2\theta = 20.0°$ [α_1 (200)] and $2\theta = 23.4°$ [α_2 (002)+(202)] corresponding to α_1 and α_2 crystalline phases [31,32]. The PHED incorporated at 10 wt % only lowered the intensity of the α_2 peak maximum, and 15 wt % of PHED lowered the intensity of both peak maxima. Since the α_1 and α_2 peak maxima represent the distance between the *anti*-parallelly aligned hydrogen-bonded PA6 chains packed in a 2D sheet-like structure and the distance between these sheets packed to form a 3D structure, respectively, it can be concluded that the presence of 10 wt % additive in the PA6/10PHED sample did not interfere with the packing of the PA6 chains into sheets but affected interactions between these sheets [33]. The increase of the additive concentration above 10 wt % influences adhesion within and between the

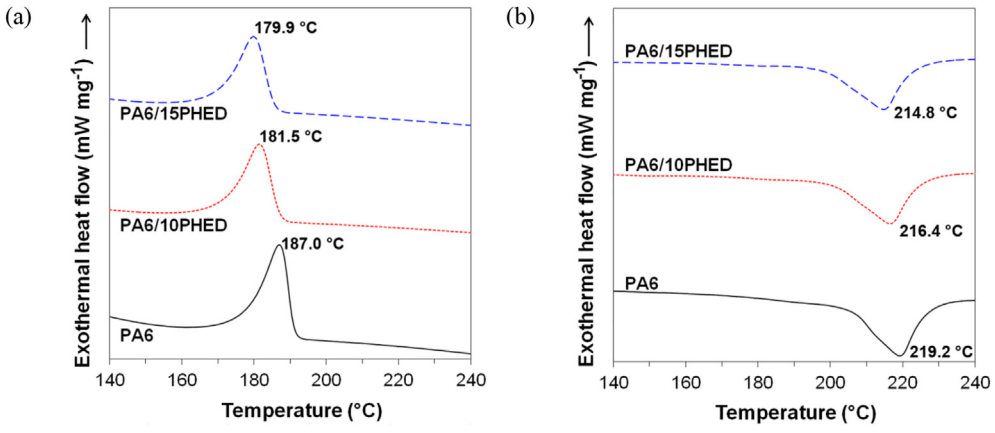

Fig. 3. (a) Crystallization temperature (T_c) from the first DSC cooling scan and (b) melting temperature (T_m) from the second DSC heating scan.

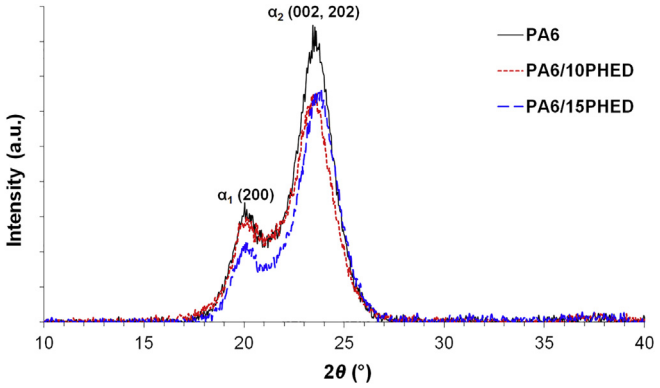

Fig. 4. XRD patterns in the range of 10°–40° for the PA6, PA6/10PHED and PA6/15PHED filament samples.

2D sheets. Considering that the concentration of the additive was 10 wt % and higher, the introduced changes in the crystalline structure are considered to be as expected.

The dynamic-mechanical properties of the PA6 and the PA6/10PHED and PA6/15PHED nanocomposite filament yarns are presented in terms of the storage modulus (*E*'), loss modulus (*E*") and loss tangent (tan δ) as functions of the temperature (Fig. 5a – c). The results show that the incorporated PHED additive, irrespective of the concentration, decreased the fiber elasticity, as reflected by lower storage modulus for the PA6/10PHED and PA6/15PHED samples compared with that of PA6 (Fig. 5a). The temperature increase lowered the storage modulus of PA6/10PHED and PA6/15PHED more quickly with respect to that of PA6. This finding suggests that the incorporated PHED in the nanocomposite caused a lack of intermolecular interactions and, consequently, facilitated the mobility of some PA6 chain segments during their transition from the glassy to the viscoelastic state.

Each relaxation transition of the storage modulus curve is accompanied by a maximum on the loss modulus curve due to the dissipation of energy as heat (Fig. 5b). PA6 showed only one relaxation transition with a maximum on the loss modulus curve at 89 °C due to α-relaxation (glass transition temperature) (Fig. 5c). The incorporated PHED in the PA6/10PHED and PA6/15PHED samples slightly decreased glass transition temperature to 86 °C and 76 °C, respectively. Because of the increased molecular segment mobility in PA6/10PHED and PA6/15PHED nanocomposites, apparent at 36 °C and 33 °C, respectively, a reduction of the elastic modulus E' is faster than for PA6 (Fig. 5a). The additional relaxation transition at about 112 °C for the nanocomposite samples resulted from the increased entropy of molecules and their tendency to achieve a thermodynamically more stable state, which molecules have failed to realize in previous relaxation phenomena.

Structural changes in the PA6 matrix due to PHED incorporation decreased the tenacity and elongation at break, indicating a reduction of the tensile properties (Fig. 5d). The later could also be affected by differences in linear densities of the partly oriented PA6, PA6/10PHED and PA6/15PHED multifilament yarns equal to 250, 300 and 280 dtex, respectively. The increased linear density resulted from changes in the viscoelastic behavior of PA6 melt due to the incorporated PHED additive (Fig. S3). The incorporated PHED additive reduced internal friction and elasticity of the polymer chains (Figs. S3a and S3b). Compared to the PA6 sample, the rheological responses of the nanocomposite PA6/10PHED and PA6/15PHED samples were characterized by lower sensitivity to the applied shear strain, which indicates a more stable system in the melted state.

3.2. Thermal stability

To gain insight into the effect of the incorporated flame retardant on PA6 decomposition, the thermal decomposition process of the PHED additive, PA6 and nanocomposite PA6/10PHED and PA6/

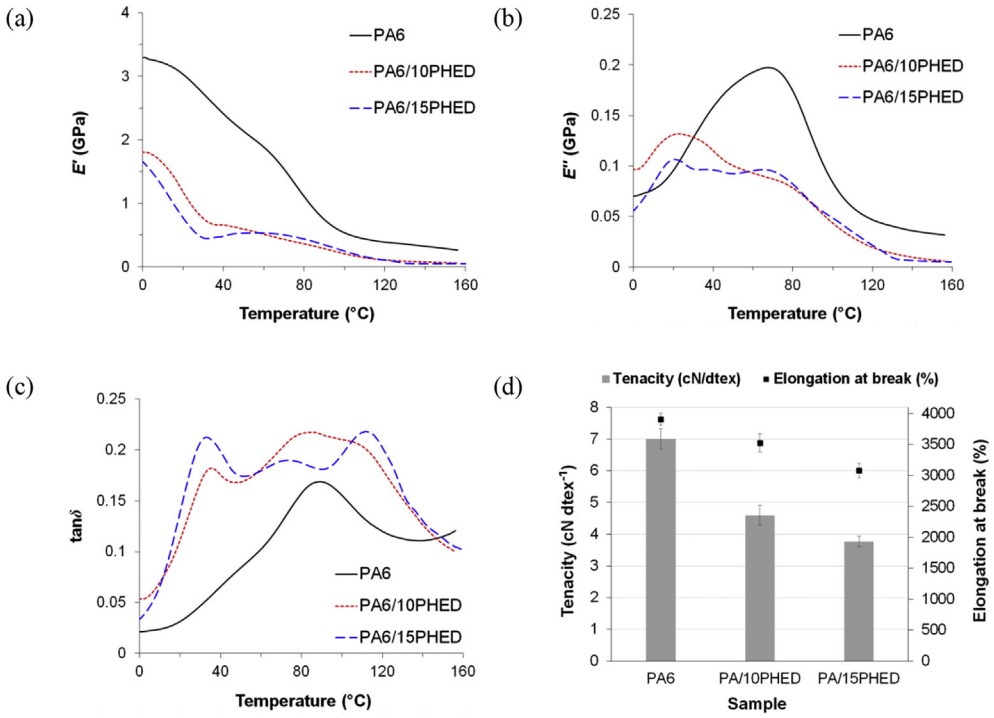

Fig. 5. (a) Storage modulus (*E*′) plotted as a function of temperature, (b) loss modulus (*E*′′) plotted as a function of temperature, (c) loss factor (tan δ) plotted as a function of temperature and (d) tensile properties of the PA6 and PA6/FR composite filaments.

15PHED filament samples in nitrogen atmosphere with simultaneous detection of the evolved gas products was analyzed by thermogravimetric analysis coupled with infrared spectrometry (TG-FTIR) (Figs. 6 and 7, and Tables S1 and S2). As seen in Fig. 6a and Table S1, the $T_{onset10\%}$ and T_{max} of the PHED additive are only a few degrees lower compared to those of the PA6 sample. According to these results, we hypothesized that PHED decomposes just before the start of PA6 decomposition. This would provide perfect timing for the PHED' radical scavengers to emerge in the gas phase and quench the radicals that sustain combustion. The results from the thermogravimetric analysis revealed that $T_{onset10\%}$ and T_{max} of the PA6/10PHED and PA6/15PHED samples were shifted to lower temperatures compared to those of the PHED and PA6 samples. Obviously, the temperature of the initial decomposition of both PA6 and PHED additive in the nanocomposite decreased compared to those of the PA6 and the PHED alone, respectively. Interactions between PA6 polymer chains and the nano-dispersed flame retardant in the nanocomposite promoted the decomposition of PHED.

Since PHED decomposes exothermically (Fig. S4), the decomposition of PA6 in the nanocomposite was promoted. Additionally, a decrease of the initial decomposition temperature of the modified polymer could be also ascribed to the interactions between decomposition products of both DOPO-based flame retardant and PA6. Namely, the acidic character of the decomposing DOPO derivative could promote the scission of the PA6 chains [15]. In order to obtain a clear view of the interactions between PA6 and PHED during pyrolysis, the weight difference curves (ΔT, presented in Fig. 6b) between experimental and calculated TG curves were determined according to the method presented by Bourbigot et al. [9,34]. The obtained negative curves confirmed that decomposing PHED additive destabilizes PA6 during the pyrolysis process.

The decomposition of the PA6 and PA6/15PHED samples in a nitrogen atmosphere was followed by the generation of ε-caprolactam, NH_3, CO_2 and H_2O, and primary aliphatic amines and hydrocarbons (Fig. 7a). The assignments of the detected FTIR bands are collected in Table S2. Compared to that of the PA6 sample, the FTIR spectrum of the PA6/15PHED sample at T_{max} and T_{max}, add showed new absorption bands, i.e., at 1510, 1339 and 750 cm^{-1}. The band at approximately 750 cm^{-1} corresponds to the stretching vibration of the *P*—C bond in the DOPO component, which confirmed the release of the phosphorus active species in the gas phase.

The other two bands at 1508 and 1339 cm^{-1} were not detected in the FTIR spectra of the PHED additive (Fig. S5). This finding indicates that FR incorporation changed the mechanism of the polyamide decomposition. This, consequently, resulted in new volatile decomposition products. The time evolution profiles for ε-caprolactam (Fig. 7b), and NH_3 and H_2O (Figs. S6 and S7), as one of the main products of PA6 decomposition, confirmed that compared to the PA6 sample, the maximum intensities of ε-caprolactam, NH_3 and H_2O corresponding to the PA6/10PHED and PA6/15PHED samples were reached within shorter times, i.e., at lower temperatures.

The thermo-oxidative decomposition of the PA6 and the PA6/10PHED and PA6/15PHED nanocomposite filament yarn samples in an air atmosphere (Fig. 8 and Table S3) confirmed that the incorporated PHED additive caused a shift of the T_{onset}, T_{max1}, and T_{max2} to lower temperatures compared to those of the PA6 (Table S3). Although PHED did not markedly influence the weight-loss rate during the first and second decomposition steps, this additive increased the residues at T_{max1} and T_{max2}.

The increased thermo-oxidative stability of the nanocomposite samples caused approximately 43% higher residue compared to that of PA6 at 500 °C. Between 500 and 800 °C, the thermo-oxidative stability of the nanocomposite samples still remained higher compared to that of PA6 but showed a gradual reduction. Therefore, the PHED additive at approximately 10 wt % concentration provided increased thermo-oxidative stability of PA6.

3.3. Vertical flammability tests

The results of the UL-94 vertical burning test are summarized in Table 1 and photographs of the bar samples subjected to the UL94 vertical burning test and cotton indicators are presented in Fig. S8. The vertical burning of the highly flammable PA6 was followed by the production of heavy flaming drips, which, although they took the flame away from the burning PA6, caused secondary ignition of the cotton indicator. Consequently, the tested PA6 polymer was classified as V-2. Without fail, the after-flame times t_1, and t_2 for the PA6/10PHED and PA6/15PHED bar samples were equal to 0 s. The corresponding melt-drips did not ignite the cotton indicators, which classified this new nanocomposite plastic material as V-0, even at 10 wt % concentration of the PHED additive. Evidently, the incorporated PHED additive successfully disrupted the ignition and flame propagation, and crucially reduced the flammability of the melt-drips.

The vertical burning behavior of the PA6 and the PA6/10PHED and PA6/15PHED fiber strand and knitted fabric samples was investigated according to the standard vertical flame spread test (ASTM D6413). The results are collected in Table 2, and charred residues and cotton indicators are shown in Fig. 9. The higher surface-to-volume ratio of fiber strands compared to the 1.2 mm-thick bar caused intensified and prolonged burning of the PA6 sample, followed by the production of smaller flaming drips, which ignited the cotton indicator (Table 2 and Fig. 9a). The incorporated PHED additive successfully provided retardation of the combustion and melt-dripping during contact with flame, and effective self-extinguishment within 2.5 ± 0.5 and 1.0 ± 0.5 s for the PA6/10PHED and PA6/15PHED fiber strand samples, respectively

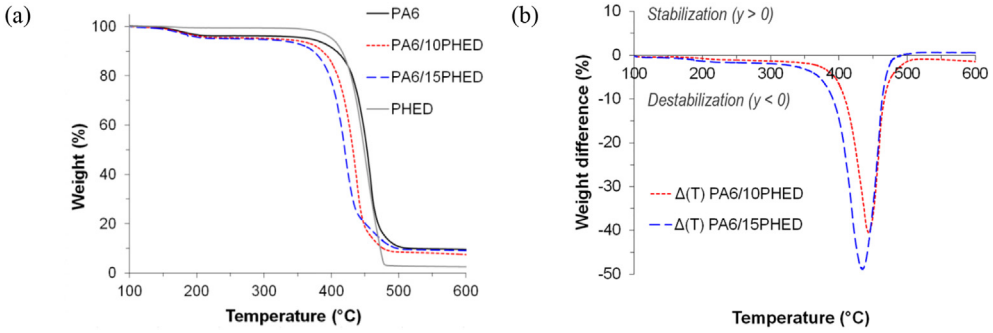

Fig. 6. (a) TG graphs of the PHED additive, PA6, and the PA6/10PHED and PA6/15PHED nanocomposite filament samples analyzed in a nitrogen atmosphere and (b) curves of the weight difference in pyrolysis.

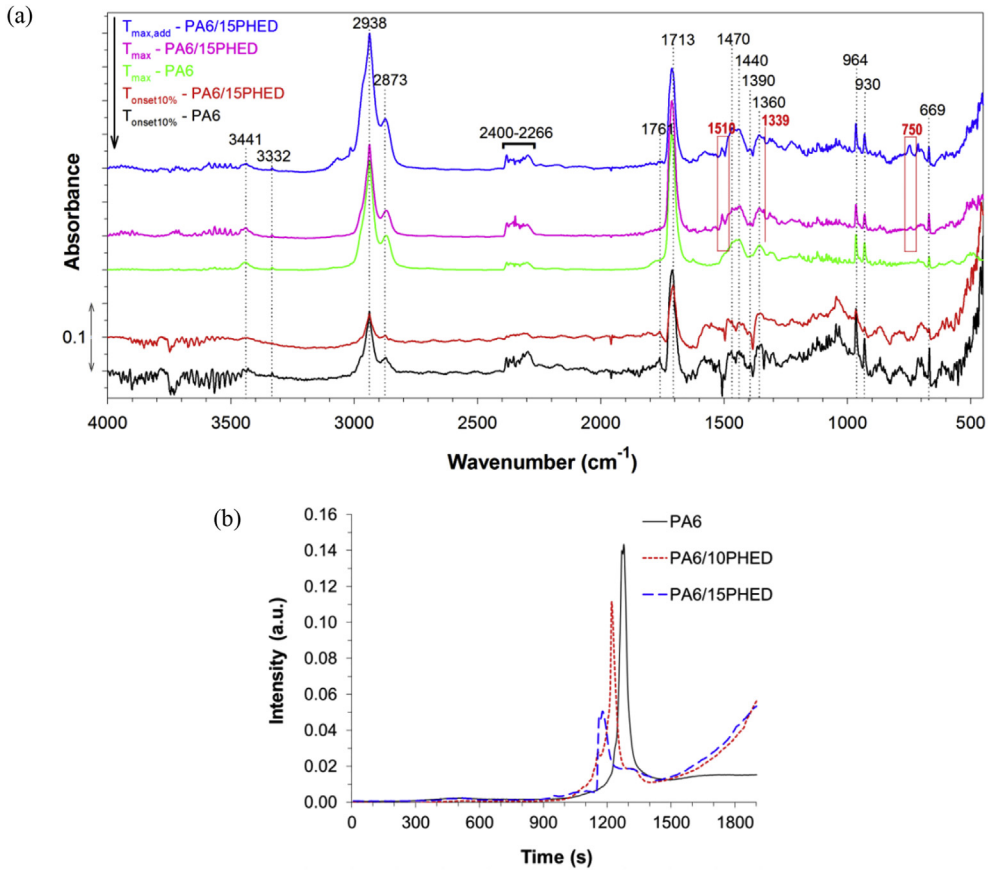

Fig. 7. (a) FTIR spectra of the gases evolved during the thermal decomposition and (b) intensity of the ε-caprolactam (1714 cm^{-1}) peak plotted as a function of decomposition time.

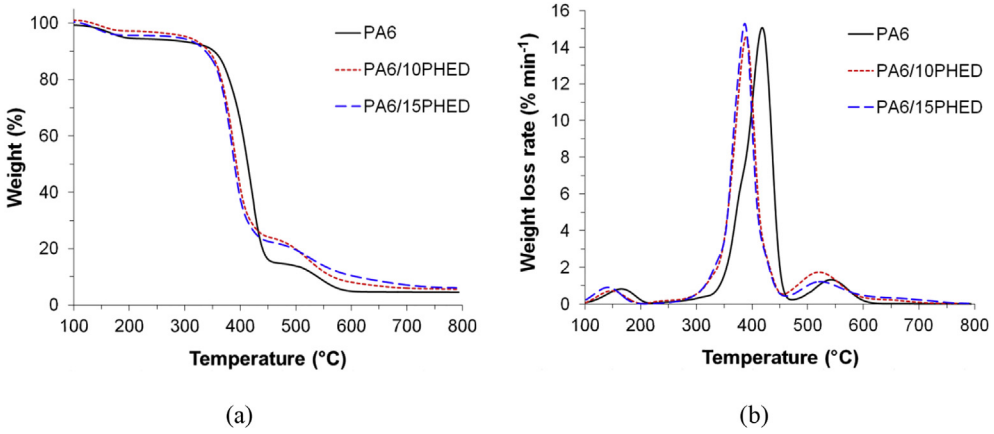

Fig. 8. (a) TG and (b) dTG graphs for the samples analyzed in air atmosphere.

Table 1
The results and classifications of the UL94 vertical flame spread tests performed on 1.2 mm-tick PA6, PA6/10PHED and PA6/15PHED bar samples.

Sample	t_1 (s)	t_2 (s)	Weight loss (%)	CI ignition	Classification
PA6	1.1 ± 0.4	0.5 ± 0.2	55 ± 5.9	Yes	V-2
PA6/10PHED	0	0	53 ± 11.1	No	V-0
PA6/15PHED	0	0	52 ± 5.2	No	V-0

(Fig. 9b and c, Movie S1). For both PA6/10PHED and PA6/15PHED, self-extinguishment occurred immediately after the first drop, followed by a significant reduction in the weight loss to 0.6 ± 0.1 and 0.5 ± 0.1%, respectively (see Table 2).

Supplementary data related to this article can be found at https://doi.org/10.1016/j.polymdegradstab.2019.05.011.

Fig. 9 The melt-dripping observed for the PA6/10PHED fiber strand sample was capable to ignite the cotton indicator, while the enhanced flame retardant action of PHED in the PA6/15PHED fiber strand sample substantially reduced the flammability of the melt drop and prevented burning of the cotton indicator. Therefore, even 10 wt % of the uniformly distributed nano-dispersed PHED additive provided effective self-extinguishment with a significant reduction

Table 2
The results of the ASTM D6143 vertical flame spread tests performed on PA6, PA6/10PHED and PA6/15PHED fiber strand and knitted fabric samples.

Sample		$t_{after-flame}$ (s)	Weight loss (%)
Fibre strand	PA6	22.0 ± 5.0	2.2 ± 0.2
	PA6/10PHED	2.5 ± 0.5	0.6 ± 0.1
	PA6/15PHED	1.0 ± 0.5	0.5 ± 0.1
Knitted fabric	PA6	14.0 ± 3.0	11.5 ± 0.8
	PA6/10PHED	6.0 ± 1.0	7.4 ± 0.1
	PA6/15PHED	1.0 ± 0.5	5.2 ± 0.5

Table 3
Smoke data collected by cone calorimetry (heat flux: 35 kW/m^2).

Sample	SEA (m^2/kg)	[CO] yield (kW/m^2)	[CO_2] yield (kW/m^2)	[CO]/[CO_2]
PA6	234 ± 1	0.010 ± 0.001	1.802 ± 0.194	0.006
PA6/10PHED	622 ± 12	0.063 ± 0.004	1.405 ± 0.080	0.045
PA6/15PHED	741 ± 13	0.081 ± 0.004	1.216 ± 0.061	0.067

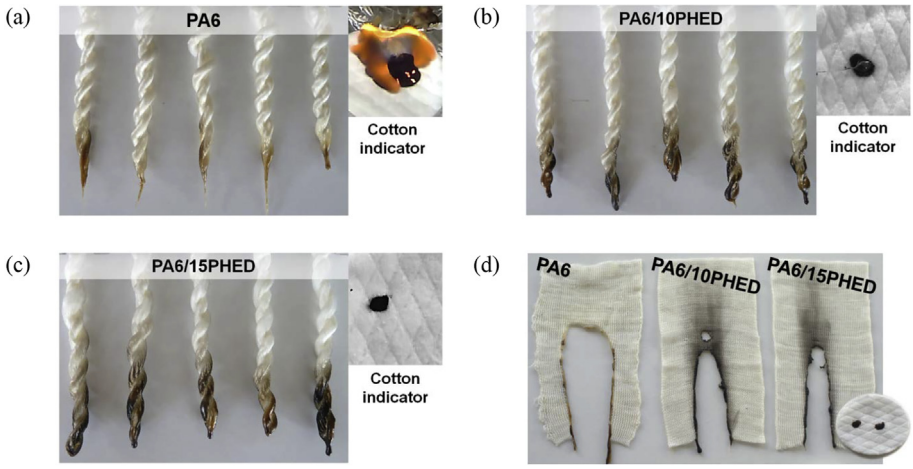

Fig. 9. Photographs of the PA6, PA6/10PHED and PA6/15PHED (a, b, c) fiber strand and (d) knitted fabric samples subjected to the ASTM D6143 vertical flame spread tests and cotton indicators.

of the after-flame time.

In the case of the knitted fabric samples, the incorporated PHED additive successfully inhibited combustion and flame spreading as well as melt-dripping during contact with flame and provided self-extinguishment within 1 s for the PA6/15PHED knitted fabric sample (Table 2 and Fig. 9d, Movies S2 and S3). To the best of the authors' knowledge, the produced halogen-free PA6/15PHED knitted fabric sample is the first-ever reported with this superior flame retardancy. As evident from Movie S3, the substantially reduced flammability of the melt drops corresponding to the PA6/15PHED sample successfully prevented burning of the cotton indicator.

Supplementary data related to this article can be found at https://doi.org/10.1016/j.polymdegradstab.2019.05.011.

3.4. Cone calorimetry tests

The resistance of the PA6, PA6/10PHED and PA6/15PHED knitted fabric samples to a heat flux of 35 kW/m^2 was assessed by cone calorimetry (Fig. 10 and Tables 3 and S4). The accelerated decomposition induced by the PHED additive decreased the TTI and did not reduce the HRR and THR. The PHED additive lowered the effective heat of combustion (EHC) of the volatiles (Table S4), which is calculated as the ratio of the heat release rate to the mass loss rate. Chemical interactions occurring in the gas phase due to the incorporated PHED additive caused a significant increase of the total smoke parameter and SEA during the combustion test (Table 3)Table S4. This finding indicates incomplete combustion. This was followed by a 10-times higher ratio between the [CO] and [CO_2] yields, which indicated that the FR gas phase-active species interfered with the oxidation of CO by OH• radicals to produce CO_2.

4. Conclusion

We have successfully produced a new-generation of halogen-free flame retardant PA6 nanocomposite filament yarns with a uniformly distributed nano-dispersed phosphorus-based FR. Here, we provided fundamental knowledge on how the physical incorporation of the meltable nano-dispersed bridged-DOPO derivative into the PA6 matrix affects the physical and mechanical properties, thermal stability and flame retardancy of this unique nanocomposite textile product. The achieved inhibition of the PA6 textile flammability demonstrate the importance of the established approach for the production of the unique nanocomposite structure with excellent processing properties, whilst the decomposition specifics of the FR maximally match those of PA6. This new production approach provides the basis for upgrading this nanocomposite system with other functional protective properties, which is crucial for the development of new-generation, sustainable, high-performance, multifunctional PA6 textile materials.

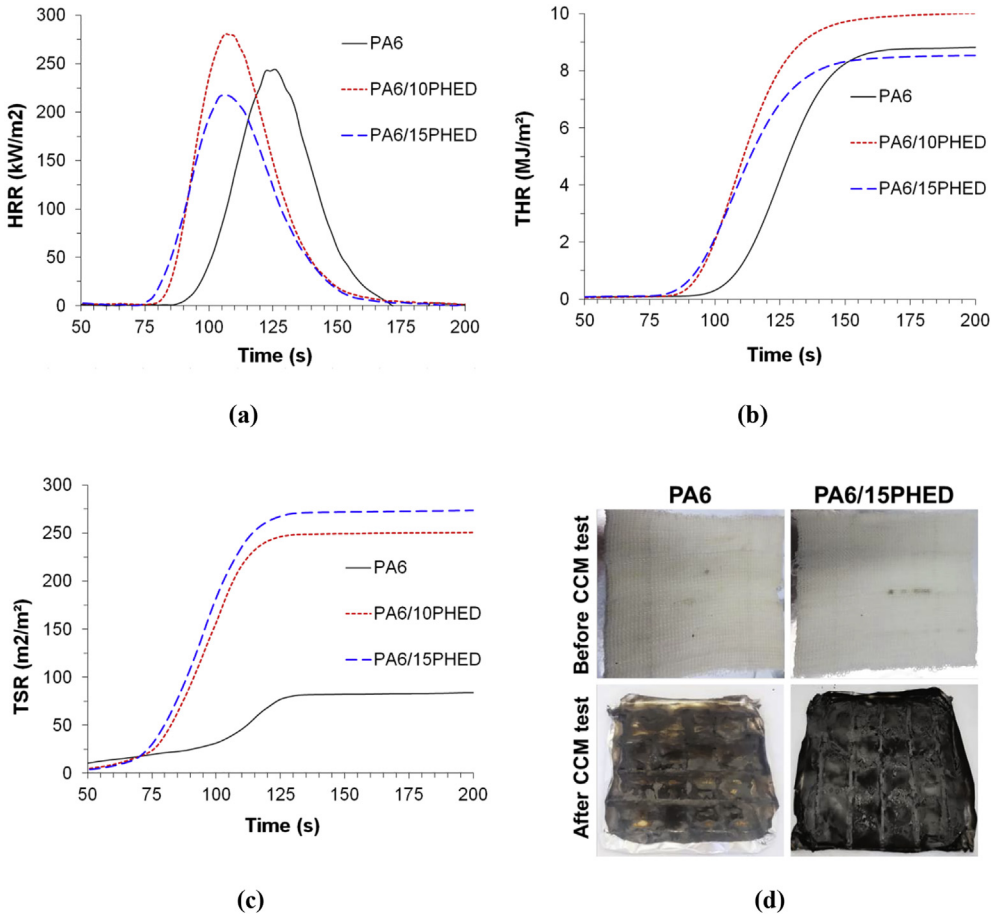

Fig. 10. (a) Heat release rate (HRR) vs. total combustion time, (b) total heat release (THR) vs. total combustion time and (c) total smoke release (TSR) vs. total combustion time for the PA6, PA6/10PHED and PA6/15PHED knitted fabric samples, and (d) photographs of the PA6 and PA6/15PHED knitted fabric samples and charred residue after cone calorimetry tests.

Acknowledgements

This work was funded by the Slovenian Research Agency, Slovenia (Basic Postdoc Project Z2-9250 and Programmes P2-0213 and P2-0393, Infrastructural Centre RIC UL-NTF). The authors would like to thank Stergar Tomaž for technical support during the melt-spinning process and Andrej Vilar for performing the knitting process.

Appendix A. Supplementary data

Supplementary data to this article can be found online at https://doi.org/10.1016/j.polymdegradstab.2019.05.011.

References

[1] M. Lewin, S.M. Atlas, Eli M. Pearce, Flame –Retardant Polymeric Materials, Plenum Press, New York, 1975.
[2] A.R. Horrocks, Technical fibres for heat and flame protection, in: A.R. Horrocks, S.C. Anand (Eds.), Handbook of Technical Textiles: Technical Textile Applications, Woodhead Publishing Cambridge, 2016, pp. 237–270.
[3] E.D. Weil, S.V. Levchik, Flame Retardants for Plastics and Textiles: Practical Applications, second ed., Hanser, Munich, 2016.
[4] M. Hong, E.Y.-X. Chen, Chemically recyclable polymers: a circular economy approach to sustainability, Green Chem. 19 (2017) 3692–3706.
[5] M.C.M. Blettler, E. Abrial, F.R. Khan, N. Sivri, L.A. Espinola, Freshwater plastic pollution: recognizing research biases and identifying knowledge gaps, Water Res. 143 (2018) 416–424.
[6] R. Horrocks, A. Sitpalan, C. Zhou, B.K. Kandola, Flame retardant polyamide fibres: the challenge of minimising flame retardant additive content with added nanoclays, Polymers 8 (2016) 288.
[7] M. Coquelle, S. Duquesne, M. Casetta, J. Sun, S. Zhang, S. Bourbigot, Investigation of decomposition pathway of polyamide 6/ammonium sulfamate fibers, Polym. Degrad. Stabil. 106 (2014) 150–157.
[8] M. Dogan, E. Bayramli, Effect of boron phosphate on the mechanical, thermal and fire retardant properties of polypropylene and polyamide-6 fibers, Fibers Polym. 14 (2013) 1595–1601.
[9] S. Bourbigot, E. Devaux, X. Flambard, Flammability of polyamide-6/clay hybrid nanocomposite textiles, Polym. Degrad. Stabil. 75 (2002) 397–402.
[10] A. Šehić, J. Vasiljević, I. Jordanov, A. Demšar, J. Medved, I. Jerman, M. Čolović, F. Hewitt, T.R. Hull, B. Simončič, Influence of N-, P- and Si-based flame retardant mixtures on flammability, thermal behavior and mechanical properties of PA6 composite fibers, Fibers Polym. 19 (2018) 1194–1206.
[11] A. Šehić, J. Vasiljević, A. Demšar, M. Leskovšek, V. Bukošek, J. Medved, M. Čolović, I. Jerman, B. Simončič, Polyamide 6 composite fibers with incorporated mixtures of melamine cyanurate, carbon nanotubes, and carbon black, J. Appl. Polym. Sci. 136 (2018) 47007.
[12] A.B. Morgan, C.A. Wilkie (Eds.), Non-Halogenated Flame Retardant Handbook, Scrivener Publishing LLC, Salem, 2014.
[13] M.M. Velencoso, A. Battig, J.C. Markwart, B. Schartel, F.R. Wurm, Molecular firefighting – how modern phosphorus chemistry can help solve the flame retardancy task, Angew. Chem. 57 (2018) 10450–10467.
[14] C. Hirsch, B. Striegl, S. Mathes, C. Adlhart, M. Edelmann, E. Bono, S. Gaan, K.A. Salmeia, L. Hoelting, A. Krebs, J. Nyffeler, R. Pape, A. Bürkle, M. Leist, P. Wick, S. Schildknecht, Multiparameter toxicity assessment of novel DOPO-derived organophosphorus flame retardants, Arch. Toxicol. 91 (2017) 407–425.
[15] A. Buczko, T. Stelzig, L. Bommer, D. Rentsch, M. Heneczkowski, S. Gaan, Bridged DOPO derivatives as flame retardants for PA6, Polym. Degrad. Stabil. 107 (2014) 158–165.
[16] W. He, H. Zhu, Y. Xiang, L. Long, S. Qin, J. Yu, Enhancement of flame retardancy and mechanical properties of polyamide 6 by incorporating an aluminum salt of diisobutylphosphinic combined with organoclay, Polym. Degrad. Stabil. 144 (2017) 442–453.
[17] J. Vasiljević, M. Čolović, I. Jerman, B. Simončič, Recent advances in production of flame retardant polyamide 6 filament yarns, Tekstilec 61 (2018) 136–148.
[18] B.L. Deopura, R. Alagirusamy, M. Joshi, B. Gupta (Eds.), Polyesters and

Polyamides, Woodhead Publishing Limited, Cambridge, 2008.
[19] R. Wang, L. Wu, D. Zhuo, J. Zhang, Y. Zheng, Fabrication of polyamide 6 nanocomposite with improved thermal conductivity and mechanical properties via incorporation of low graphene content, Ind. Eng. Chem. Res. 57 (2018) 10967–10976.
[20] Q. Xu, P. Hu, D. Wu, X. Li, Z. Zhang, Studies on the mechanical and friction properties of polyamide 6-Cu/Si nanocomposites, J. Macromol. Sci., Pure Appl. Chem. 54 (2017) 323–327.
[21] P. González-Morones, E. Hernández-Hernández, S. Fernández-Tavizón, R. Ledezma-Rodríguez, A. Sáenz-Galindo, G. Cadenas-Pliego, C.A. Ávila-Orta, R.F. Ziolo, Exfoliation, reduction, hybridization and polymerization mechanisms in one-step microwave-assist synthesis of nanocomposite nylon-6/graphene, Polymer 146 (2018) 73–81.
[22] Y. Zheng, R. Wang, X. Dong, L. Wu, X. Zhang, High strength conductive polyamide 6 nanocomposites reinforced by prebuilt three-dimensional carbon nanotube networks, ACS Appl. Mater. Interfaces 10 (2018) 28103–28111.
[23] A.B. Morgan, C.A. Wilkie (Eds.), Flame Retardant Polymer Nanocomposites, John Wiley & Sons, Inc., Hoboken, 2007.
[24] G.C. Alfonso, G. Costa, M. Pasolini, S. Russo, A. Ballistreri, G. Montaudo, C. Puglisi, Flame-resistant polycaproamide by anionic polymerization of ε-caprolactam in the presence of suitable flame-retardant agents, J. Appl. Polym. Sci. 31 (1986) 1373–1382.
[25] T. Kurauchi, A. Okada, T. Nomura, T. Nishio, S. Saegusa, R. Deguchi, R. Degushi, Nylon 6-clay hybrid - synthesis, properties and application to automotive timing belt cover, SAE Tech. Pap (1991) 910584. https://doi.org/10.4271/910584.
[26] Z.-Y. WU, W. XU, J.K. XIA, Y.-C. LIU, Q.-X. WU, W.-J. XU, Flame retardant polyamide 6 by in situ polymerisation of ε-caprolactam in the presence of melamine derivatives, Chin. Chem. Lett. 19 (2008) 241–244.
[27] Y. LI, Y. LIN, K. SHA, R. XIAO, Preparation and characterisation of flame retardant melamine cyanurate/polyamide 6 composite fibres via in situ polymerisation, Textil. Res. J. 87 (2017) 561–569.
[28] L. Long, J. Yin, W. He, S. Qin, J. Yu, Influence of a phenethyl-bridged DOPO derivative on the flame retardancy, thermal properties, and mechanical properties of poly(lactic acid), Ind. Eng. Chem. Res. 55 (2016) 10803–10812.
[29] W. Yan, J. Yu, M. Zhang, S. Qin, T. Wang, W. Huang, L. Long, Flame-retardant effect of a phenethyl-bridged DOPO derivative and layered double hydroxides for epoxy resin, RSC Adv. 7 (2017) 46236–46245.
[30] Q. Yao, H. Zhou, W.W. Zhang, W.H. Cao, Z.X. Liu, Z. Xu, DOPO Derivatives as Well as Preparation Method and Application Thereof, China Patent, 2014. CN104086593.
[31] Y. Chen, D. Li, W. Yang, C. Xiao, Enhancement of mechanical, thermal and tribological properties of AAPS-modified graphene oxide/polyamide 6 nanocomposites, Compos. B Eng. 138 (2018) 55–65.
[32] T. Kashiwagi, R.H. Harris, X. Zhang, R.M. Briber, B.H. Cipriano, S.R. Raghavan, W.H. Awad, J.R. Shields, Flame retardant mechanism of polyamide 6–clay nanocomposites, Polymer 45 (2004) 881–891.
[33] N. Sanjeeva Murthy, Hydrogen bonding, mobility, and structural transitions in aliphatic polyamides, J. Polym. Sci., Part B: Polym. Phys. 44 (2006) 1763–1782.
[34] S. Bourbigot, T. Turf, S. Bellayer, S. Duquesne, Polyhedral oligomeric silsesquioxane as flame retardant for thermoplastic polyurethane, Polym. Degrad. Stabil. 94 (2009) 1230–1237.